*Electrochemical and Solid-State Letters,* **9** (7) A344-A348 (2006)
1099-0062/2006/9(7)/A344/5/$20.00 © The Electrochemical Society

# Quantification of Liquid Water Saturation in a PEM Fuel Cell Diffusion Medium Using X-ray Microtomography

**Puneet K. Sinha,[a,*] Philip Halleck,[b] and Chao- Yang Wang[a,**,z]**

[a]*Electrochemical Engine Center and Department of Mechanical and Nuclear Engineering, and* [b]*Energy Institute and Department of Energy and Geo-Environmental Engineering, The Pennsylvania State University, University Park, Pennsylvania 16802, USA*

Quantification of liquid water saturation distribution in a diffusion medium is critical to establishing a basic understanding of the two-phase flow and flooding occurrence in proton exchange membrane (PEM) fuel cells. We have used X-ray microtomography to obtain high-resolution ($10 \times 10 \times 13.4$ μm), three-dimensional images of liquid water distribution in a gas diffusion layer (GDL) during gas purge. We report on temporally resolved liquid saturation profiles across the GDL thickness and demonstrate the feasibility of using X-ray microtomography to quantify liquid water distribution at the component level. The results show that the drying rate decreases exponentially with purge time and no significant liquid water removal takes place after 6 min of purge, at room temperature.
 [DOI: 10.1149/1.2203307] 

Manuscript submitted February 17, 2006; revised manuscript received March 16, 2006. Available electronically May 10, 2006.

The importance of water management in a proton exchange membrane (PEM) fuel cell has been stressed widely in the literature.[1,2] There is a great need to quantitatively measure liquid water saturation in porous layers such as gas diffusion layer (GDL), microporous layer (MPL), and catalyst layer (CL), as this is a key parameter in flooding occurrence under normal operations as well as ice formation during cold start of PEM fuel cells. The water present in these porous layers, at shutdown, may freeze under subzero temperatures and makes cold start of a PEM fuel cell difficult. In practice, a fuel cell is typically purged with inert gas such as nitrogen before shutdown to remove the liquid water from it. Quantification of liquid water inside the GDL, during the purge process, can provide significant insight into the purge mechanisms and cold start characteristics of PEM fuel cells.

Unfortunately, the need to quantitatively measure liquid water saturation in the porous layers of a fuel cell has yet to be addressed. Prior measurements of liquid water distribution in PEM fuel cells have included optical visualization using transparent fuel cells,[3-5] neutron radiography,[6-9] and magnetic resonance imaging (MRI).[10-12] Optical visualization is focused primarily on channel two-phase flow and clogging as well as liquid water distribution on the surface of GDL. Neutron radiography provides a two-dimensional map of liquid water and hence can neither distinguish between the liquid water present in various components of a fuel cell nor resolve the liquid water saturation distribution along the thickness of the GDL. In general, neutron radiographs quantify the liquid water under the assumption that all the liquid water is present in the cathode GDL only. Such an assumption may not be accurate under various operating conditions. MRI is used to visualize the transport of liquid water across a polymer electrolyte membrane. However, the presence of magnetically inductive materials like carbon makes MRI unsuitable for quantifying liquid water in GDL. Recent developments in microscale visualization techniques offer new opportunities for imaging pore-scale flow and multiphase transport in porous media. In recent years, X-ray microtomography has been used widely in soil science and petroleum industry to obtain structural information such as porosity and pore topology and to image fluid transport in reservoir rocks.[13-17]

In the present work, we have quantitatively studied the distribution of liquid water saturation inside the GDL during gas purge. The main objective of this study is to assess the feasibility of using X-ray microtomography to quantify liquid water saturation in porous layers of a PEM fuel cell.

* Electrochemical Society Student Member.
** Electrochemical Society Active Member.
z E-mail: cxw31@psu.edu

## X-Ray Microtomography

X-ray microtomography (micro CT) is an extension of a medical imaging technique called X-ray computed tomography, more commonly known as CT scanning. Computed tomography (CT) provides a high-resolution 3D map of the variation of X-ray adsorption within a sample. Such a variation in X-ray adsorption may result from the presence of different phases/elements in the sample or from heterogeneous density. Voxel sizes in a micro CT commonly are at a level of 10 μm or smaller with special equipment. The main features of X-ray microtomography are described here briefly. A detailed description of the basics of X-ray microtomography can be found in Ref. 18-20.

When a material is exposed to an X-ray beam, the intensity of X-ray is attenuated as it traverses through the material. The transmitted radiation is received by an array of detectors. The intensity of X-rays gets attenuated as it passes through the material and the degree of attenuation is given by Beer–Lambert's law for monochromatic beam

$$\frac{I}{I_o} = \exp(-\mu x) \qquad [1]$$

where $I_o$ is the intensity of the unattenuated X-ray beam, $I$ the beam's intensity after it traverses a thickness of $x$ in the material, and $\mu$ the linear attenuation coefficient, which depends on both electron density and atomic number. Usually, it is not practical to reference behavior to the X-ray attenuation coefficient $\mu$. Instead, CT numbers are used and defined as

$$CT = A\left(\frac{\mu_{\text{material}} - \mu_{\text{air}}}{\mu_{\text{ref}} - \mu_{\text{air}}}\right) - B \qquad [2]$$

where $\mu_{\text{material}}$, $\mu_{\text{air}}$, and $\mu_{\text{ref}}$ are linear attenuation coefficients of the scanned material, air and a reference material, respectively. $A$ and $B$ are constants called gain and offset respectively. For industrial scanning, $A$ and $B$ are arbitrary and the reference material is chosen to best match the subject at hand. Choice of reference material and constants A and B does not affect the final result, as it is simply a matter of scaling the data. In the present work, $A$ is equal to 100 and $B$ is taken as 2048.

The average $CT$ number of a scanned GDL can be correlated to the liquid water saturation by simple proportionality

$$CT = CT_{\text{air}}\varepsilon(1 - s) + CT_{\text{w}}\varepsilon s + CT_{\text{s}}(1 - \varepsilon) \qquad [3]$$

where $\varepsilon$ and $s$ are the porosity and the liquid water saturation in the scanned voxel of GDL. $CT_{\text{air}}$, $CT_{\text{w}}$, and $CT_{\text{s}}$ represent the $CT$ numbers for air, water, and solid matrix, respectively. So, for a dry and completely saturated GDL the average $CT$ numbers are given, respectively, by

$$CT_{dry} = CT_{air}\varepsilon + CT_s(1 - \varepsilon) \quad [4]$$

$$CT_{wet} = CT_w\varepsilon + CT_s(1 - \varepsilon) \quad [5]$$

The parameter $CT_s$ can be eliminated from the calculation by subtracting every scanned image from the respective image of a dry GDL. Subtracting the scan when the GDL is completely saturated with that of the dry GDL yields

$$CT_{wet} - CT_{dry} = (CT_w - CT_{air})\varepsilon \quad [6]$$

The variation in liquid water saturation can be found by subtracting the scan at a particular time from that of the completely saturated GDL scan

$$CT - CT_{wet} = -(CT_w - CT_{air})\varepsilon(1 - s) \quad [7]$$

where $CT$ and $s$ are the average $CT$ number and liquid saturation in a scanned voxel, respectively. Hence liquid water saturation in the GDL can be given by the following equation

$$s = \frac{CT - CT_{dry}}{CT_{wet} - CT_{dry}} \quad [8]$$

The X-ray microtomography technique is also capable of quantifying the liquid water distribution at the pore level given a sufficient spatial resolution (i.e, smaller than the pore size).

## Experimental

The experimental setup consists of an X-ray CT imaging system, the OMNI-X HD600, a GDL holder, vacuum suction and gas flow system. The vacuum suction line is attached to the top part of the GDL holder. The GDL holder is in vertical orientation and a schematic representation of assembly with axis of rotation is shown in Fig. 1a. GDL is placed on the top of parallel gas channels with dimensions of $1 \times 1$ mm, typically used in PEM fuel cells, machined in the bottom part of the GDL holder shown in Fig. 1b. For the present study, a 200 $\mu$m thick Toray carbon paper with 10.24 $\times$ 10.24 mm area was used.

The GDL holder was rotated 360° in the X-ray beam while the two-dimensional array of detectors provides the attenuated views to data acquisition computer. The computer system reconstructs multiple "slices" or cross-sectional image, of attenuated values, that represent the spatial variation of CT number. In the present work, entire GDL was scanned in 15 slices along the thickness of the GDL, with the voxel dimension of $10 \times 10 \times 13.4$ $\mu$m. Here, 13.4 $\mu$m is the thickness of each slice.

During each experiment, the GDL was first scanned in dry state, and then vacuum was applied to the top surface of GDL and liquid water allowed to flow into the GDL from the bottom. After complete saturation, the vacuum suction line and liquid water line were closed and the GDL was again scanned in the fully saturation state. These two scans provide the reference points to convert the CT number of a partially saturated GDL scan into a map of the liquid water saturation, according to Eq. 8. Note that this calibration is performed voxel by voxel by using the two reference points locally.

The GDL was then purged by flowing nitrogen at room temperature along the gas channels at 5 L/min. To provide a saturation history, the GDL was rescanned periodically during the purge procedure.

## Results and Discussion

As mentioned above, the GDL was scanned in 15 slices parallel to its thickness. Reconstructed images of the spatial distribution of liquid water in the GDL at different time intervals were obtained. Figure 2 shows the reconstructed image of a slice in the middle of GDL during the purge. In the following, purge dynamics are discussed based on the liquid water saturation variation with time for this middle slice in GDL.

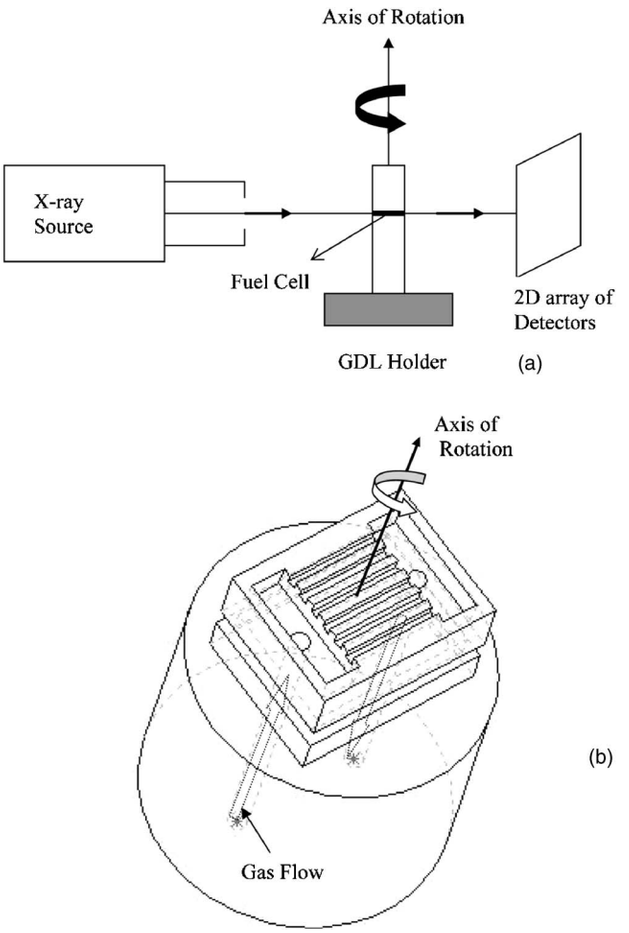


**Figure 1.** (a) Schematic of the experimental setup. (b) Schematic of the lower part of GDL holder where the flow field is composed of parallel gas channels.

1. Figure 3a was obtained by subtracting the vacuum-saturated images of the GDL from the dry image. The gray color represents liquid water and the black color shows the presence of air.

2. Figure 3b was obtained by subtracting the images obtained after 2 min of purge from the vacuum-saturated image. The black color shows the area from where liquid water has been replaced by nitrogen after 2 min of purging. The gray shows the area where liquid saturation is not changed during 2 min of purge. The presence of white shows the portion of GDL that was initially (at the vacuum saturated state) filled with air and at the end of 2 min of purge, was filled with liquid water.

3. Figure 3c shows the additional water removed from the GDL after an additional 4 min of purge. Again black color is the result of additional water removal between 2 min and 6 min of purge process, whereas the gray color shows the portion of the GDL where saturation had not changed. The area from where liquid water has been removed in the first 2 min of purge appears gray.

4. Figure 3d shows liquid water removal from the GDL between 6 and 12 min of purge process. As seen from the figure, only a very small amount of liquid water has been removed from GDL in this time interval.

5. Figure 3e shows the liquid water removal between 12 and 25 min of purge process. Almost no water has been removed in this time interval of purge process. Fig. 3f compares the saturation inside GDL after 25 min of purge with that of dry GDL, and apparently GDL becomes almost dry after 25 min of purge process.

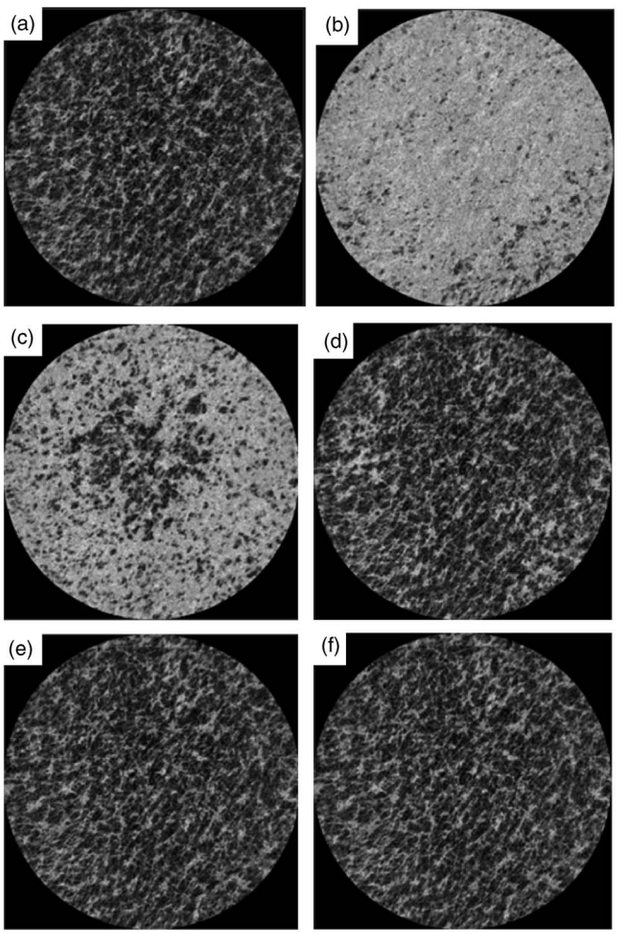


**Figure 2.** Reconstructed images for the middle slice of GDL: (a) in dry state, (b) pre-saturated with liquid water, (c) after 2 min of purge, (d) after 6 min of purge, (e) after 12 min of purge, and (f) after 25 min of purge.

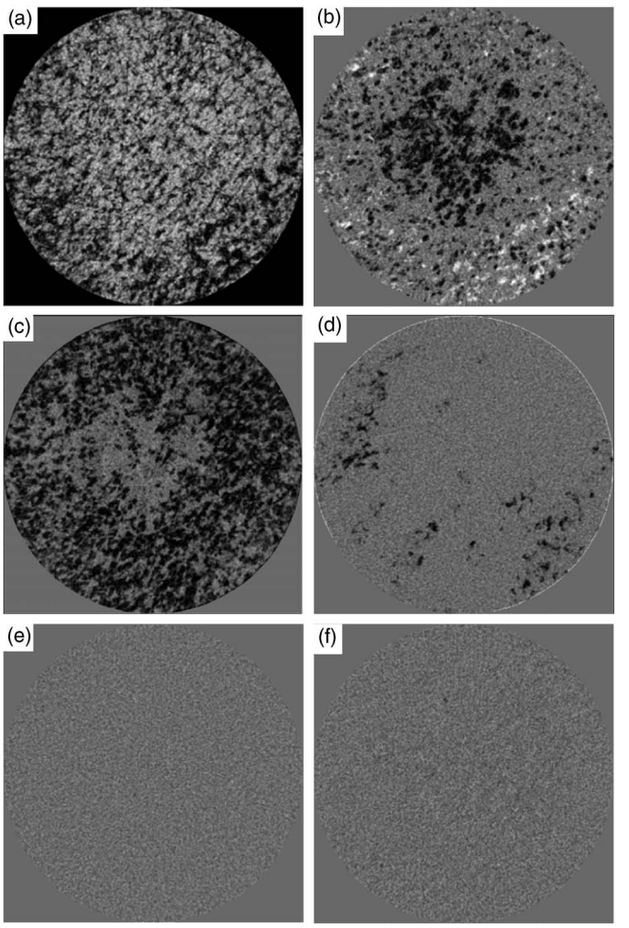


**Figure 3.** Subtracted images of the middle slice in the GDL. (a) Vacuum saturated image subtracted from the image in the dry state. (b) After 2 min of purge subtracted from the vacuum saturated image. (c) After 6 min of purge subtracted from the image after 2 min of purge. (d) After 12 min of purge subtracted from the image after 6 min of purge. (e) After 25 min of purge subtracted from the image after 12 min of purge. (f) After 25 min of purge subtracted from the image in the dry state.

Figure 4 shows the liquid saturation profiles across the thickness of GDL with purge time. Liquid saturation distribution is plotted for the inner seven slices out of the 15 scanned slices in the GDL because of ring artifacts present in the GDL slices near the top and bottom edge of the GDL holder. Ring artifacts arise due to abrupt change in density and atomic number at the interface of Toray carbon paper and GDL holder. As seen from Fig. 4, liquid saturation decreases quickly during the first 6 min of the purge process but then slows.

A high-resolution, three-dimensional map of liquid water saturation in the inner seven slices of GDL was obtained using the image analysis software, ImageJ.[21] First, a volume was rendered using the stack of the inner seven slices and then cut diagonally to see the liquid water clusters along the thickness direction. Figure 5 shows the distribution of liquid water along the thickness direction after vacuum saturation and 2 min of purge. The white color in the GDL portion shows liquid water whereas black color shows air. For clarity, a top view of rendered volume along with the cutting plane is shown in the inset. Similar high resolution, three-dimensional maps of liquid water saturation were obtained for later stages of purge and can be found in Ref. 22. As seen from these figures, initially the liquid water forms a connected cluster that spans the entire GDL. As the drying front moves into the GDL, it erodes the liquid cluster and produces isolated liquid water clusters. The liquid water can be removed from such disconnected clusters only by evaporation. Because, in the present experiments, the GDL holder and the nitrogen gas are at the same temperature, evaporation is not a dominant water removal mechanism. This decreases the water removal rate.

## Conclusions

We have explored the possibility of using X-ray microtomography to quantify liquid water distribution in a PEM fuel cell. Liquid water saturation distributions along the GDL thickness were obtained as a function of time for a gas purge process. It was found that liquid water saturation in the GDL can be quantified with sufficient resolution using X-ray microtomography and three-dimensional liquid water saturation maps can provide important insight into the transport of liquid water in GDL. A detailed investigation of purge process and effect of various operating parameters on it using X-ray microtomography is ongoing and will be published in the future.

Table I compares the X-ray imaging to neutron imaging and MRI. As shown from Table I, X-ray microtomography is uniquely suited to quantify the liquid water saturation in porous layers of a PEM fuel cell. We plan to investigate liquid water transport and related phenomena in an operating fuel cell using X-ray microtomography.

The ability of X-ray microtomography in resolving samples $\sim 10$ $\mu$m thick opens exciting possibilities to quantify liquid water

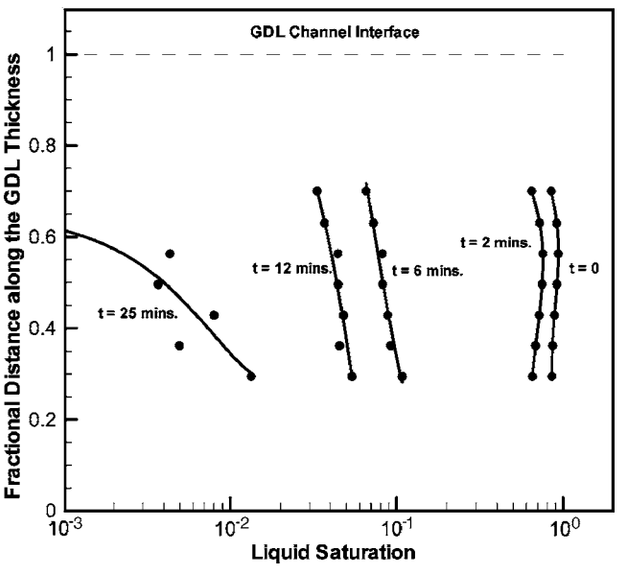


**Figure 4.** Variation of liquid water saturation along the thickness of GDL at different purge times.

**Table I. Comparison of several techniques for quantifying liquid water in a PEM fuel cell**

| | X-ray imaging | Neutron imaging | MRI |
|---|---|---|---|
| Sensitivity to water | Sensitive | Extremely sensitive | Extremely sensitive |
| Spatial resolution | | | |
| Present | 10 μm | 100-150 μm | 25 μm |
| Future | 1 μm | 10-50 μm | 10 μm |
| Temporal resolution (for a single image: radiograph or shadowgraph) | 0.07 s | 0.03 s | 50 s |
| Disadvantages for fuel cell research | ✓Less sensitivity to water | ✓Complex and costly technique<br>✓Low spatial resolution prevents its use in MPL and CL | ✓Requires absence of magnetically inductive materials, e.g., carbon<br>✓Unsuitable for CL, MPL and GDL due to the presence of carbon<br>✓Low spatial and temporal resolution |

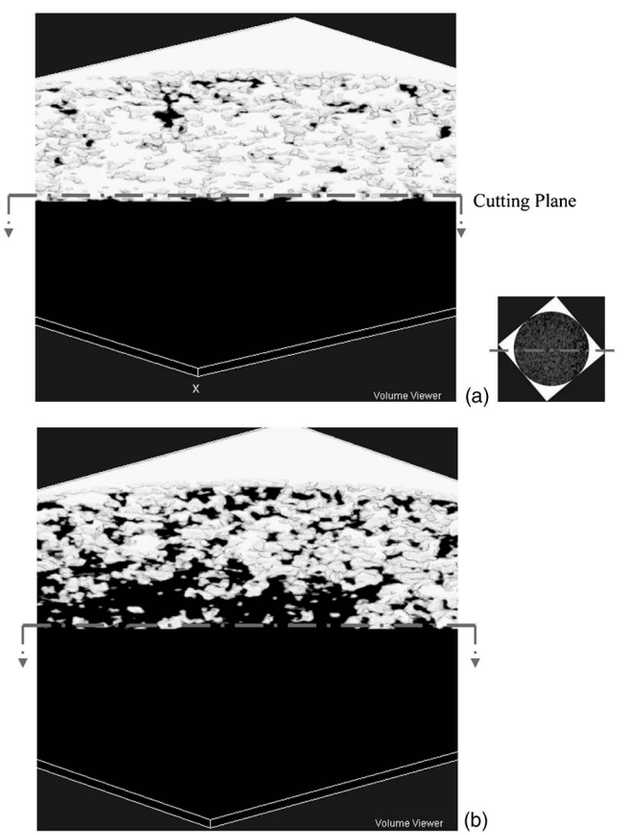


**Figure 5.** Liquid water distribution across the thickness of GDL shown by cutting the rendered volume diagonally. (a) After vacuum saturation. (b) After 2 min of purge. Top view of the rendered volume formed from the inner seven slices in the GDL is shown in the inset. The GDL portion between the front edge and the cutting plane is removed to show the liquid water clusters in the thickness direction.

saturation in the catalyst layer (~10 μm) as well as in the MPL (30–50 μm). However, despite its initial promise, X-ray microtomography technique requires much more development and refinement for the application to fuel cells. Presently, ring artifacts are observed in the top and bottom slices, which are in contact with the GDL holder. Slices with these artifacts cannot be used for further image processing; hence measures must be devised to eliminate or reduce these artifacts. In the present study, results were presented here with a voxel size of 13.4 μm in the thickness direction. A further improvement in the resolution of X-ray microtomography down to 1–5 μm is preferred in quantitative studies of liquid water distribution in catalyst layer and MPL.

## Acknowledgment

We are thankful to Dr. Richard Steinberger for designing the experimental setup and helping to carry out the experiments.

*The Pennsylvania State University assisted in meeting the publication costs of this article.*

## References

1. U. Pasaogullari and C. Y. Wang, *J. Electrochem. Soc.*, **151**, A399 (2004).
2. C. Y. Wang, *Chem. Rev. (Washington, D.C.)*, **104**, 4727 (2004).
3. K. Tüber, D. Pócza, and C. Hebling, *J. Power Sources*, **124**, 403 (2003).
4. X. G. Yang, F. Y. Zhang, A. Lubawy, and C. Y. Wang, *Electrochem. Solid-State Lett.*, **7**, A408 (2004).
5. F. Y. Zhang, X. G. Yang, and C. Y. Wang, *J. Electrochem. Soc.*, **153**, A225 (2006).
6. A. B. Geiger, A. Tsukada, E. Lehmann, P. Vontobel, A. Wokaun, and G. G. Sherer, *Fuel Cells*, **2**, 92 (2003).
7. R. Satija, D. L. Jacobson, M. A. Arif, and S. A. Werner, *J. Power Sources*, **129**, 238 (2003).
8. D. Kramer, J. Zhang, R. Shimoi, E. Lehmann, A. Wokaun, K. Shinohara, and G. G. Scherer, *Electrochim. Acta*, **50**, 2603 (2005).
9. N. Pekula, K. Heller, P. A. Chuang, A. Turhan, M. M. Mench, J. S. Brenizer, and K. Ünlü, *Nucl. Instrum. Methods Phys. Res. A*, **542**, 134 (2005).
10. S. Tsushima, K. Teranishi, and S. Hirai, *Electrochem. Solid-State Lett.*, **7**, A269 (2004).
11. K. Teranishi, S. Tsushima, and S. Hirai, *J. Electrochem. Soc.*, **153**, A664 (2006).
12. K. Feindel, S. H. Bergens, and R. E. Wasylishen, *ChemPhysChem*, **7**, 67 (2006).
13. F. M. Auzerias, J. Dunsmuir, B. B. Ferreol, N. Martys, J. Olsen, T. S. Ramakrishnan, D. H. Rothman, and L. M. Schwartz, *Geophys. Res. Lett.*, **23**, 705 (1996).
14. P. Spanne, K. W. Jones, L. D. Prunty, and S. H. Anderson, in *Tomography of Soil-Water-Root Processes*, S. H. Anderson and J. W. Hopmans, Editors, p. 43, SSSA Madison, WI.

15. D. Wildenschild, J. W. Hopmans, M. L. Rivers, and A. J. R. Kent, *Vadose Zone J.*, **4**, 112 (2005).
16. M. E. Coles, R. D. Hazlett, P. Spanne, W. E. Soll, E. L. Muegge, and K. W. Jones, *J. Pet. Sci. Eng.*, **19**, 55 (1998).
17. J. Liu, A. Polak, D. Elsworth, and A. Grader, *J. Contam. Hydrol.*, **78**, 53 (2005).
18. S. R. Stock, *Int. Mater. Rev.*, **44**, 141 (1999).
19. R. A. Ketchman and W. D. Carlson, *Comput. Geosci.*, **27**, 381 (2001).
20. D. Wildenschild, J. W. Hopmans, C. M. P Vaz, M. L. Rivers, D. Rikard, and B. S. B. Christensen, *J. Hydrol.*, **267**, 285 (2002).
21. W. S. Rasband, ImageJ, National Institutes of Health, Bethesda, MD, http://rsb.info.nih.gov/ij/, 1997–2004.
22. P. K. Sinha, P. Halleck, and C. Y. Wang, Penn State University Electrochemical Engine Center Report No. 2005-07 (2005).